Line intensities for the $\nu 6$ and $2\nu 3$ bands of methyl iodide (12CH3I)

F. Kwabia-Tchana, Y. Attafi, L. Manceron, D. Doizi, J. Vander Auwera, A. Perrin

Line intensities for the ν_6 and $2\nu_3$ bands of methyl iodide ($^{12}CH_3I$)

F. KwabiaTchana,[a] Y. Attafi,[a,b] L. Manceron,[c,d] D. Doizi,[e] J. Vander Auwera,[f] A. Perrin[g]

[a] Laboratoire Interuniversitaire des Systèmes Atmosphériques (LISA), UMR CNRS 7583, Université Paris Est Créteil et Université Paris Diderot, Institut Pierre Simon Laplace, 61 avenue du Général de Gaulle, F-94010 Créteil Cedex, France.

[b] Laboratoire de Dynamique Moléculaire et Matériaux Photoniques, Université de Tunis, Ecole Nationale Supérieure d'Ingénieurs de Tunis, 5 Av Taha Hussein, 1008 Tunis, Tunisia.

[c] Ligne AILES, Synchrotron SOLEIL, L'Orme des Merisiers, St-Aubin BP48, F-91192 Gif-sur-Yvette Cedex, France.

[d] Sorbonne Université, CNRS, MONARIS, UMR 8233, 4 place Jussieu, F-75005 Paris, France

[e] DEN-Service d'Etude du Comportement des Radionucléides (SECR), CEA, Université Paris-Saclay, F-91191 Gif-sur-Yvette, France

[f] Service de Chimie Quantique et Photophysique, C.P. 160/09, Université Libre de Bruxelles, 50 avenue F.D. Roosevelt, B-1050 Brussels, Belgium.

[g] Laboratoire de Météorologie Dynamique/IPSL, UMR CNRS 8539, Ecole Polytechnique, Université Paris-Saclay, RD36, F-91128 PALAISEAU Cedex, France.

Nb of figures: 6

Nb of Tables: 4

Corresponding author: Agnes Perrin, Agnes.Perrin@lmd.polytechnique.fr

Abstract

The goal of this study is to measure for the first time absolute line intensities for the ν_6 band of methyl iodide (CH_3I) centered at 892.918 cm^{-1}. High-resolution Fourier transform spectra were recorded at various pressures for the whole 500 – 1450 cm^{-1} spectral range. Using these spectra, a large set of CH_3I individual line intensities was measured for the ν_6 band. These experimental intensities were least squares fitted to derive the expansion of the ν_6 transition moment operator. The theoretical model used to describe the line positions and intensities accounts for the hyperfine structure in the 6^1 and ground states and for the vibration-rotation resonances that couple the 6^1 energy levels with those of the 3^2 and 2^1 vibrational states [A. Perrin *et al.*, J. Mol. Spectrosc. 324 (2016) 28 – 35]. As the $2\nu_3$ band is extremely weak, its associated transition moment operator was estimated from band strength available in the literature. A comprehensive list of line positions and intensities was generated for the ν_6 and $2\nu_3$ bands of CH_3I at 11 µm, which should be useful for the possible detection of this species by the future IASI-NG satellite instrument (Infrared Atmospheric Sounding Interferometer New Generation), now under preparation (https://iasi-ng.cnes.fr/en/IASI-NG/index.htm).

Keywords: **methyl iodide; CH_3I; high-resolution Fourier transform spectroscopy; Coriolis resonances; line positions; line intensities; hyperfine structure**

A. Introduction

The goal of the present study is to generate a list of spectroscopic line parameters for methyl iodide (CH_3I) in the 11 µm region. This work focuses on line intensities for the ν_6 band of $^{12}CH_3I$ and follows our previous investigation that concerned line positions for the same band [1]. Although absent in the public access spectroscopic databases such as HITRAN (http://hitran.org/) [2] or GEISA [3], this band located at 892.916 cm^{-1}, coincides with the 11 µm transparency window of the atmosphere [4] and could therefore be a good candidate for the detection of atmospheric CH_3I, for example, by the future IASI-NG satellite instrument

(Infrared Atmospheric Sounding Interferometer New Generation), now under preparation (https://iasi-ng.cnes.fr/en/IASI-NG/index.htm).

Status of the ν_6 line positions for $^{12}CH_3I$

As far as the line positions are concerned, methyl iodide was the subject of numerous studies. Only the literature relevant to the present investigation and the $^{12}CH_3I$ isotopic species will be described here. A more complete review can be founded elsewhere [1, 5-13].

Relying on Fourier transform spectra, Alanko *et al.* [9], Paso and Alanko [10], and Haykal et al. [13] performed a very detailed analysis of the $2\nu_3$ and ν_6 bands of $^{12}CH_3I$ and identified a large set of transitions in both bands. However, assignments in the ν_6 band were complicated by the existence of hyperfine structures resulting from the large ^{127}I iodine nuclear quadrupole moment (nuclear spin I = 5/2). These hyperfine splittings are easily observable for ν_6 transitions involving J values not much larger than K ($J \leq 2\times K$). The energy level calculations performed by Paso and Alanko [10] accounted explicitly for the weak first-order Coriolis resonance coupling the 6^1 and 3^2 energy levels, while the hyperfine structure was accounted for by a perturbative treatment. Later, Carocci *et al.* performed a new investigation of the rotational structure of the ground and 6^1 vibrational states of $^{12}CH_3I$ using a Doppler-free double resonance technique [12]. The results of these rotational measurements were combined with a large set of literature data obtained by microwave techniques [5, 6, 8, 12] and from infrared investigations of the ν_6 band [10] to get complete sets of rotational and hyperfine parameters for both the ground and the 6^1 excited states of $^{12}CH_3I$ [12]. However, the existence of a 6^1 and 3^2 Coriolis resonance was not mentioned in this latter study [12], and therefore not accounted for explicitly. Finally, our recent and extensive investigation [1] of the ν_6 and $2\nu_3$ bands of $^{12}CH_3I$ was performed using high resolution spectra recorded using Bruker IFS125HR Fourier transform spectrometers (FTS) available at the AILES beamline of the SOLEIL Synchrotron facility and at LISA in Créteil (France). The assignment procedure and linelist calculation performed in that work explicitly considered the hyperfine structure for the ν_6 and $2\nu_3$ bands using literature values of the nuclear quadrupole and spin rotational constants in the ground, $\left(6^1;\ell=1\right)$ and $\left(3^2;\ell=0\right)$ states [8,12]. A large set of 6^1 and 3^2 experimental rotational energy levels was deduced from the observed rotational or hyperfine transitions, after removing from the latter the contribution of the individual line shift due to

the hyperfine structure. These levels were satisfactorily reproduced using an effective Hamiltonian model involving the $\{6^1, 3^2, 2^1\}$ interacting states, thus accounting for the weak Coriolis type resonances coupling the 6^1 energy levels with those of the $\left(3^2;\ell=0\right)$ and $\left(2^1;\ell=0\right)$ states. Indeed, for series involving rather high rotational quantum numbers, additional Coriolis resonances coupling the $\left(6^1;\ell=1\right)$ and $\left(2^1;\ell=0\right)$ energy levels were observed for the first time [1]. Note that our recent study [1] investigated the strong ν_6 band only, considering the ν_2 band as a "perturber" of the ν_6 band. An extended analysis using an effective model that involved the $\left\{\left(2^1;\ell=0\right),\left(3^16^1;\ell=1\right),\left(5^1;\ell=1\right)\right\}$ interacting states, thus including the ν_2 band, had been performed in the frame of the very thorough investigation of the $\nu_2/\nu_5/\nu_3+\nu_6$ band system of $^{12}CH_3I$ and $^{13}CH_3I$ [11].

Status of the ν_6 line intensities for $^{12}CH_3I$

To the best of our present knowledge, line intensity measurements were never carried out for the ν_6 or $2\nu_3$ bands of $^{12}CH_3I$. Measurements of low-resolution band intensities have however been reported for the six fundamental bands of $^{12}CH_3I$ [14,15], and absorption cross sections have been measured at Pacific Northwest National Laboratory (PNNL) [16]. *Ab initio* computed band intensities have been reported for $^{12}CH_3I$ by Schneider and Thiel [17].

B. Experimental procedure and wavenumbers calibration

B.1. Experimental procedure

Seven absorption spectra of methyl iodide have been recorded in the range from 500 to 1450 cm^{-1} using the high-resolution Bruker IFS125HR FTS located at the LISA facility in Créteil (France). The instrument was equipped with a silicon carbide Globar source, a KBr/Ge beamsplitter and a liquid nitrogen cooled HgCdTe (MCT) detector. An optical filter with a bandpass of 500 – 1450 cm^{-1} was to improve the signal-to-noise ratio. The FTS was continuously evacuated below 3×10^{-4} hPa by a turbomolecular pump to minimize absorption by atmospheric gases. The diameter of the entrance aperture of the spectrometer was set to 1.5 mm to maximize the intensity of infrared radiation falling onto the MCT detector without saturation or loss of spectral resolution. Interferograms were recorded with a 40 kHz scanner frequency and a maximum optical path difference (MOPD) of 473.68 cm. According to the

Bruker definition (resolution = 0.9/MOPD), this corresponds to a resolution of 0.0019 cm^{-1}. The spectra were obtained by Fourier transformation of the interferograms using a Mertz phase correction with a 1 cm^{-1} resolution, a zero-filling factor of 2 and no apodization (boxcar option).

The sample was purchased from Sigma Aldrich (FlukaChemie GmbH, 99% purity) and used without further purification. For all the measurements, the sample was contained in a Pyrex glass cell providing an absorption path length of 12.4 ± 0.1 cm and equipped with wedged ZnSe anti-reflection coated windows. The sample pressure in the cell was measured using calibrated MKS Baratron capacitance manometers models 628D (13.332 hPa full scale) and 627D (133.32 hPa full scale) characterized by a stated reading accuracy of 0.12%. Considering the uncertainty arising from small variations of the pressure during the recording (~ 0.35%), we estimated the measurement uncertainty on the pressure to be equal to 0.5%. All the spectra were recorded at a stabilized room temperature of 295 ± 1 K.

The following procedure was used to record the spectra. A background spectrum was first collected while the cell was being continuously evacuated. It was recorded at the same resolution as the sample spectra to ensure proper removal of the H_2O or CO_2 absorption lines and of the weak channeling generated by the ZnSe cell windows. The infrared gas cell was then passivated several times with the CH_3I sample. Finally, spectra were recorded for seven different sample pressures of methyl iodide. The seven pressures chosen and the number of interferograms recorded and averaged to yield the corresponding spectra are listed in Table 1. All the sample spectra were ratioed against the empty cell background spectrum. The root mean square (RMS) signal-to-noise ratio (S/N) in the ratioed spectra ranged between 100 and 300.

B.2. Wavenumbers calibration

The spectra were calibrated by matching the measured positions of about 25 lines of residual CO_2 observed therein to reference wavenumbers available in HITRAN [2] with a RMS deviation of 0.00013 cm^{-1}. The absolute accuracy of the measured CH_3I line positions was estimated as the square root of the sum of squares of the accuracy of the reference CO_2 line positions in HITRAN (better than 0.0001 cm^{-1}) plus twice the RMS deviation between the observed frequencies and values listed in HITRAN2016 for CO_2, yielding in total 0.00028 cm^{-1}.

C. Line intensity measurements

C.1. Retrieval of line intensities

The line intensities were measured using a multi-spectrum fitting program developed in Brussels [18, 19]. This program adjusts spectroscopic (e.g. line positions, intensities and widths) and spectrum-specific (e.g. baseline) parameters to best-fit synthetic spectra to the observed spectra using a Levenberg-Marquardt non-linear least squares fitting procedure. Each synthetic spectrum, interpolated 4 times with respect to the observed spectrum, is calculated as the convolution of the molecular transmission spectrum with an instrument line shape function, which includes the effects of the finite maximum optical path difference and of the finite source aperture diameter of the interferometer. In the present work, no distortion of the instrument line shape was observed: the nominal aperture diameter of 1.5 mm was therefore retained in the simulated spectra. The background in each spectrum was represented by a polynomial expansion up to the second order (a constant or an affine function was however found sufficient in most cases), and the profile of the lines was modeled using a Voigt function [20] with Gaussian width always held fixed to the value calculated for the Doppler broadening. The measurements were carried out on small spectral intervals, ranging from 0.11 to 0.7 cm^{-1} and containing one to several lines, and involved the simultaneous fitting of all the spectra. For the line intensity measurements, we selected carefully the transitions for which the hyperfine structure is not observable: this means that the hyperfine broadening is weaker that the Doppler line width. The fitted line parameters were the positions, intensities and self-broadening coefficients (assumed to be proportional to the pressure of methyl iodide). Self-shift of the lines was ignored. The required initial values of the positions and intensities of lines belonging to the ν_6 band of methyl iodide considered in the present work were generated from our previous frequency analysis [1]. The self-broadening coefficient of all the lines was initially set to 0.2 cm^{-1} atm^{-1}. Figure 1 presents an example of the results of a fit. It involved 14 lines observed in the spectral range 915.3 to 915.8 cm^{-1}, pressures ranging from 3.406 to 28.70 hPa and a total of 44 fitted parameters. The upper and lower panels show the observed spectra and best-fit residuals, respectively. The absence of signatures out of the spectral noise in the residuals suggests that the Voigt profile is appropriate to fit the observed lines, whose S/N are about 100, as in the region presented in figure 1.

C.2. Uncertainty analysis

Examination of the residuals of the fits shows that they are generally less than 1%. However, to estimate the accuracy of the measured intensities requires considering the uncertainties on the physical parameters, contributions from possible systematic errors [21] as well as the uncertainties derived from the fits, taken as the standard deviation. The various sources of error considered in the present work and their associated uncertainties expressed relative to the line intensities are given in Fig. 2 for 3 selected strong, medium and weak lines, representative of the 840 measured lines, i.e. ${}^{R}R(26,0)$, ${}^{P}P(30,4)$ and ${}^{P}P(57,4)$. Figure 2 shows that systematic errors and the standard deviations of the fits are the main sources of error. The dominant contributions to the systematic errors were found to arise from the location of the full-scale (100%) photometric level, electronic and detector nonlinearities. Baseline offset results in a corresponding intensity uncertainty. The effect of noise and small offset in these have been discussed in previous works [21]. The 0% level could be checked readily and the 100% level fitted on the spectra in regions without absorptions. An arbitrary, but conservative estimate of 2% of the line intensities has been retained here. For the 840 measured transitions, the average relative uncertainty on the line intensities is 1.5%. For each transition, we then calculated an upper limit for the overall uncertainty based on the maximum uncertainty of the individual experimental parameters, i.e. ε_{si} (sample purity), ε_{t} (temperature), ε_{p} (pressure), ε_{pl} (pathlength), ε_{fit} (standard deviation from fit) and ε_{sys} (systematic errors), assuming that these uncertainties are uncorrelated:

$$\varepsilon = \sqrt{\varepsilon_{si}^2 + \varepsilon_{t}^2 + \varepsilon_{p}^2 + \varepsilon_{pl}^2 + \varepsilon_{fit}^2 + \varepsilon_{sys}^2} \qquad \text{Eq. (1)}$$

Using this equation and the experimental relative uncertainties involved, the estimated overall uncertainty (estimated accuracy) for each of the 840 line intensities measured was calculated. These uncertainties ("Unc") are provided in Table 2. On average, the estimated accuracy for line intensities is equal to 3%.

D. <u>Line intensity calculations</u>

The integrated absorption cross section $k_{\tilde{\nu}}^{N}$ [in $cm^{-1}/(molecule\ cm^{-2})$] of a line of CH_3I in natural abundance corresponding to a transition between a lower level L of energy E_L and an upper level U of energy E_U can be expressed as [2]:

$$k_{\tilde{\nu}}^{N} = I_a \frac{8\pi^3\tilde{\nu}}{4\pi\varepsilon_0 3hc}\frac{1}{Z(T)} g_{nucl}^{I}.g_{nucl}^{H}\left(1-\exp\left(-\frac{hc\tilde{\nu}}{kT}\right)\right)\exp\left(-\frac{hcE_L}{kT}\right)R_L^U \qquad \text{Eq. (2)}$$

In Eq. (2), T is the temperature (in Kelvin), $\tilde{\nu}=(E_U-E_L)/hc$ is the line position (in cm^{-1}), I_a = 0.98896 (8) is the isotopic abundance of $^{12}CH_3I$ [22], and g_{nucl}^{I} and g_{nucl}^{H} are the statistical weights of the lower level respectively resulting from the iodine (I = 5/2) and hydrogen (I = 1/2) nuclear spins. For $^{12}CH_3I$, g_{nucl}^{H} = 4, irrespective of the A_1:A_2:E symmetries. As pointed out previously, the hyperfine structure due to the iodine quadrupole interaction may be observable for transitions involving low J values as compared to K, complicating measurements of individual line intensities. Therefore, the present least squares fit calculation only considered experimental intensities measured for lines free of any observable hyperfine structure. For such transitions, g_{nucl}^{I} = 6 for all levels.

$Z(T) = Z_{vib}(T)\times Z_{rot}(T)$ is the total internal partition function, written as the product of vibrational and rotational contributions. The vibrational part, $Z_{vib}(T)$, was computed in the Harmonic Oscillator Approximation (HOA) using the vibrational frequencies available in the literature [1, 7, 11, 23,24]. In this approximation, the $Z_{vib}(T)$ and the rotational contribution,,$Z_{rot}(T)$ are assumed independent. $Z_{rot}(T)$, was calculated using the ground state rotational levels computed up to J=90 with the constants quoted in Ref. [12] and accounting for the nuclear spin statistical weights provided here above. The values of the rotational, vibrational and total partition functions thus calculated between 70 and 400 K are listed in Table A1 (available as supplementary material).

The present work only deals with cold bands originating from the CH_3I non-degenerate ground state ($0;\ell=0$), identified as |0> in the following. In Eq. (2), R_L^U is the square of the matrix element of the transformed dipole moment operator μ_Z', which takes the following form:

$$R_L^U = \left|\left\langle (v';\ell'),J'K'\left|\mu_Z'\right|0,J''K''\right\rangle\right|^2 \qquad \text{Eq. (3)}$$

$(v';\ell')$ are the vibrational quantum numbers in the upper state, which belongs to the $\{(6^1;\ell=1),(3^2;\ell=0),(2^1;\ell=0)\}$ set of interacting states. *J"K"* and *J'K'* are the rotational

quantum numbers in the ground state and in the upper levels of the transition, respectively. The expansions of the $\left|\left(v';\ell'\right),J'K'\right\rangle$ and $\left|0,J''K''\right\rangle$ upper and lower state rovibrational wavefunctions, which depend on the symmetry (A_1, A_2 or E) of the considered energy level, are given in Eqs. (1) to (2) of Ref. [25]. Finally, the dipole moment operator $\mu_Z^{'}$ can be expanded as follows:

$$\mu_Z^{'} = \sum_{v'\in B'} \left|0\right\rangle {}^{v'}\mu_Z^{\Delta\ell} \left\langle v';\ell'\right| \qquad \text{Eq. (4)}$$

where ${}^{v'}\mu_Z^{\Delta\ell}$ is the transformed dipole moment operator corresponding to the transition $|0\rangle \rightarrow |v';\ell'\rangle$. As ν_6 transitions access the 6^1 upper vibrational state involved in the $\left\{\left(6^1;\ell=1\right),\left(3^2;\ell=0\right),\left(2^1;\ell=0\right)\right\}$ triad of interacting states, the transition moment operators of the parallel $2\nu_3$ and ν_2 bands also contribute to the ν_6 line intensities, together with their ν_6 counterpart. For the ν_6 $\Delta\ell=\pm1$ perpendicular band, the expansion of the transformed transition dipole moment operator can be written as:

$${}^{6}\mu_Z^{\Delta\ell=1} = {}^{6}\mu_0^{\Delta\ell=1}\varphi_x + {}^{6}\mu_4^{\Delta\ell=1}\left\{i\varphi_y, J_z\right\} + {}^{6}\mu_5^{\Delta\ell=1}\left\{\varphi_z, iJ_y\right\} \qquad \text{Eq. (5)}$$

This expression is an extension of the asymmetric-top molecules model [26]. Written in the phase convention of Refs. [27-29], it does not differ formally from the approach used in Refs. [28,29]. In Eq. (5), φ_x , φ_y , and φ_z are the Z_x, Z_y, and Z_z components of the direction cosines between the Z laboratory fixed axis and the *x*, *y* and *z* molecular axes, and ${}^{6}\mu_q^{\Delta\ell=1}$ is the q^{th} parameter in the expansion of ${}^{6}\mu_Z^{\Delta\ell=1}$. Because of the absence of information on a possible centrifugal distortion dependence of the line intensities in the $2\nu_3$ and ν_2 bands, the expansion of the transition moment operators of the parallel $2\nu_3$ and ν_2 bands, ${}^{33}\mu_Z^{\Delta\ell=0}$ and ${}^{2}\mu_Z^{\Delta\ell=0}$ respectively, was restricted to its 0-th order term:

$${}^{33}\mu_Z^{\Delta\ell=0} = {}^{33}\mu_0^{\Delta\ell=0}\varphi_z \qquad \text{Eq. (6a)}$$

$${}^{2}\mu_Z^{\Delta\ell=0} = {}^{2}\mu_0^{\Delta\ell=0}\varphi_z \qquad \text{Eq.(6b)}$$

In Eq. (5), operators with the ($\Delta\ell = \pm 1; \Delta K = \pm 1$) selection rules are only considered for the ν_6 perpendicular band while the zero-order term in Eq. (6) corresponds to the ($^{\Delta\ell = 0}$;$\Delta K = 0$) rule for the $2\nu_3$ or ν_2 parallel bands. Indeed, it proved useless to account in the expansion of the ν_6, $2\nu_3$ or ν_2 transition moment operators for higher order terms. Some of these symmetry-allowed [28, 29] terms involve different $(\Delta\ell; \Delta K)$ selection rules than those considered in Eqs. (5) and (6).

As already stated, individual line intensities are not available for the $2\nu_3$ or ν_2 parallel bands. In spite of this, the relative strengths of the $\nu_6/2\nu_3/\nu_2$ bands can be estimated to equal 1/0.0126/2.352 (±10%) using the existing experimental band intensities [16]. The zero-order terms in the expansion of the $\nu_6/2\nu_3/\nu_2$ transition moment operators are therefore in the following ratio (in absolute values):

$$\left|{}^{6}\mu_0^{\Delta\ell=\pm1}\right| / \left|{}^{33}\mu_0^{\Delta\ell=0}\right| / \left|{}^{2}\mu_0^{\Delta\ell=0}\right| \approx 1/0.122/1.53\ (\pm 10\%) \qquad \text{Eq. (7)}$$

The set of 840 line intensities measured for the ν_6 band was introduced in least squares fit calculations to determine the parameters involved in the expansion of ${}^{6}\mu_{Z}^{\Delta\ell=1}$ [Eq. (5)]. As the Coriolis resonances between the 6^1, 3^2 and 2^1 vibrational levels only result in local perturbations involving a strong band (ν_6) and weak bands ($2\nu_3$ or ν_2), the question is whether or not the $2\nu_3$ or ν_2 transition moment operators contribute significantly to the intensities of the ν_6 band. Three sets of computations were therefore performed. The first two involved setting the ν_2 and $2\nu_3$ bands transition moment zero order parameters (i.e. ${}^{2}\mu_{0}^{\Delta\ell=0}$ and ${}^{33}\mu_{0}^{\Delta\ell=0}$, respectively) in turn to the value predicted from ${}^{6}\mu_{0}^{\Delta\ell=\pm1}$ as discussed here above, while the last computation was done setting ${}^{2}\mu_{0}^{\Delta\ell=0}$ and ${}^{33}\mu_{0}^{\Delta\ell=0}$ to zero. It appeared that these three computations do not differ significantly from each other, either in terms of the quality of the fit or in the values of the derived ${}^{6}\mu_{q}^{\Delta\ell=1}$ parameters. This could be expected because the set of 840 experimental ν_6 line intensities used for the present calculation does not include lines affected by the Coriolis resonances involving ν_2 and $2\nu_3$. The latter lines were indeed too weak to be observed. It was therefore decided to perform the final computation of the line intensities setting the ν_2 transition moment operator to zero and the ${}^{33}\mu_{0}^{\Delta\ell=0}$ parameter to the fixed value ${}^{33}\mu_{0}^{\Delta\ell=0} \approx 0.122 \times {}^{6}\mu_{0}^{\Delta\ell=\pm1}$ deduced as described here above. The resulting values of the ${}^{6}\mu_{q}^{\Delta\ell=\pm1}$ and ${}^{33}\mu_{0}^{\Delta\ell=0}$ parameters are quoted in Table 2, together with the statistical analysis of the line intensity computation. Figure 3 gives an overview of the results of the calculation, while the complete list of measured and calculated line intensities is provided in Table A2 (available as supplementary material).

E. <u>Synthetic spectrum</u>

A comprehensive list of line positions and intensities (at 296 K) was generated for the ν_6 and $2\nu_3$ bands of $^{12}CH_3I$ using the vibrational energies, the rotational and coupling constants given in Table 7 of Ref. [1] for the upper interacting states and the rotational constants provided in Ref. [12] for the ground state, together with the values of the ${}^{6}\mu_{q}^{\Delta\ell=\pm1}$ and ${}^{33}\mu_{0}^{\Delta\ell=0}$

transition moment constants given in Table 2. The calculations were performed for a "pure" isotopic sample of $^{12}CH_3I$ using an intensity cut off of $2x10^{-26}cm^{-1}$/(molecule cm^{-2}). This list is provided as supplementary material of this article. Table 3 provides some details on this linelist.

As already mentioned, the large values of the ^{127}I iodine nuclear quadrupole moment leads to easily observable hyperfine structures for ν_6 transitions involving $J \leq 2\times K$ (such a splitting is much smaller for parallel bands such as $2\nu_3$). A given [J', K'] – [J", K"] vibration-rotation transition of the ν_6 or $2\nu_3$ band is split into several hyperfine components with F" = J"±1/2, J"±3/2, J"±5/2 and $\Delta F = \pm 1$. The theoretical methods used to account for these effects are well described in the literature [30,31]. In the present work, the shift $^{Hyp}\delta$ = ([J', K', F'] – [J", K", F"]) – ([J', K'] – [J", K"]) of the position of a given [J', K', F'] – [J" K", F"] hyperfine component relative to the position of its [J', K'] – [J", K"] counterpart was computed using the semi-perturbative treatment described in Ref. [1]. The line intensity of each hyperfine component was deduced from its corresponding [J', K'] – [J", K"] hyperfine-free vibration-rotation transition by replacing in Eq. (1) $g^I_{nucl} = 6$ by $^{J'F'}_{J"F"}g^I_{nucl}$ with [30]:

$$ {}^{J'F'}_{J"F"}g^I_{nucl} = (2F'+1)(2F"+1)\begin{Bmatrix} J' & F' & 5/2 \\ F" & J" & 1 \end{Bmatrix}^2 \qquad \text{Eq. (8)} $$

Obviously, summation over F' and F" leads to $\sum_{F'F"} {}^{J'F'}_{J"F"}g^I_{nucl} = 6$.

However, accounting for the hyperfine structure increases dramatically the size of the linelist for the ν_6 and $2\nu_3$ bands. To limit the size of the linelist, the detailed hyperfine structure was generated only when it proved necessary for the correct modeling of the CH_3I spectrum at 11 µm.

For the present linelist, we decided to account for the hyperfine structure provided it leads to a $^{Hyp}\delta$ hyperfine shift larger (in absolute value) than a pre-defined ^{Hyper}Limit threshold limit of 0.002 cm^{-1}. This lower limit more or less corresponds to the observed width of the lines in the experimental spectra studied in this work, involving the combined contributions from the Doppler width [γ_D (half width at half maximum) ~ 0.0005 cm^{-1} at T = 296 K in the studied spectral region], from pressure broadening [32] and from the experimental line shape of the FTS.

F. Validation of the line intensity calculation

Detailed comparisons of observed and calculated spectra were already presented on Figs. 1 to 6 of Ref. [1]. Another detailed comparison is shown in Fig. 4. It is clear that for low J values, accounting for the hyperfine structure leads to a better agreement between the observed and calculated spectra.

The results of the present line intensity study can also be compared with the existing low-resolution band intensity measurements. Table 4 lists the integrated band intensities S_{band} measured [15], determined from measured absorption cross sections [16] or calculated *ab initio* [17]. Integrated band intensities include contributions from isotopic species other than $^{12}CH_3I$ and from various hot bands. Comparison of these integrated band intensities with the sum of the individual calculated line intensities reported in the present work therefore require application of the following empirical expression [33]

$$S_{band} \approx Z_{Vib}(T) \sum_k S_k \qquad \text{Eq. (9)}$$

where S_k is the intensity of line k in the linelist established for a pure isotopic sample of $^{12}CH_3I$ which is described in section E. Eq. (9) assumes that the intensities of the ν_6 band of all isotopologues of methyl iodine are the same, which seems to be reasonable as the ν_6 band is only weakly perturbed. The integrated intensities of the ν_6 and $2\nu_3$ bands thus obtained for the present work, i.e. $S(\nu_6) \approx 1.38\times10^{-18}$ cm^{-1}/(molecule cm^{-2}) (±15%) and $S(2\nu_3) \approx 2.04\times10^{-20}$ cm^{-1}/(molecule cm^{-2}) (±20%), are also given in Table 4. It can be noted that the present line intensity measurements lead to an integrated band intensity in the ν_6 region (750 – 1025 cm^{-1}) that is about 8% smaller than the values reported by Dickson *et al.* [15] and Sharpe *et al.* [16]. This result will have to be checked by future line intensity studies. The *ab initio* prediction for the ν_6 band intensity [17] is about twice as large as the experimental values [14, 15]. However, recent computations performed for CH_3Cl [34, 35] clearly indicate that the quality of *ab initio* predictions was significantly improved since 1987.

Figures 5 and 6 compare the PNNL (Pacific Northwest National Laboratory) absorption cross sections with the results of the present calculations for the ν_6 and $2\nu_3$ bands, respectively. As detailed in Ref. [16], PNNL absorption cross sections are for a sample (CH_3I in the present case) diluted in 1 atm of nitrogen at 296 K and were derived from Fourier transform spectra recorded at a resolution of 0.112 cm^{-1} (0.9/MOPD). As methyl iodide exhibits significant self-broadening, some of the sharper lines are actually broader than instrumental limits. To account for the hot bands contribution, our calculated line intensities were multiplied by $Z_{Vib}(296K) = 1.1158$. The comparison of Fig. 5 clearly shows that, on average, our computed intensities (cold ν_6 and hot bands) are weaker that the PNNL intensities by a factor of about 1.087. A closer look at the residuals (not shown) indicate that the signatures observed result from contributions from hot bands and possible line mixing effects.

G. Conclusion

In this work, individual line intensities were measured for the first time for the ν_6 band of $^{12}CH_3I$. Using a theoretical model that accounts for the resonances coupling the 6^1 energy levels with those of the 3^2 and 2^1 vibrational states, it was possible to determine the transition moment operator of the ν_6 band. The transition moment of the very weak $2\nu_3$ band was determined using the integrated intensity of the band, estimated from the absorption cross sections measured at Pacific Northwest National Laboratory [16]. A linelist was generated for the ν_6 and $2\nu_3$ bands, accounting for the hyperfine structure when it proved necessary. Comparisons with integrated band intensities and absorption cross sections available in the literature show that the present line intensities are about 8% lower.

ACKNOWLEDGEMENTS

The DECA-PF project is sponsored by the French government `Investments for the future' program through the grant ANR-11-RSNR-0003 supervised by the French National Research Agency (ANR) under the `Research in Nuclear Safety and Radioprotection' (RSNR) research initiative.

References

[1] Perrin A, Haykal I, Kwabia Tchana F, Manceron L, Doizi D, Ducros G. New analysis of the ν_6 and $2\nu_3$ bands of methyl iodide (CH_3I). J Mol Spectrosc 2016;324:28-35.

[2] Gordon IE, Rothman LS, Hill C, Kochanov RV, Tana Y, Bernath PF, Birk M,Boudon V, Campargue A, Chance KV,Drouin BJ, Flaud JM, Gamache RR, Hodges JT, Jacquemart D, Perevalov VI, Perrin A, Shine KP, Smith MA, Tennyson J, Toon GC, Tran H, Tyuterev VG, Barbe A,Császár AG, Devi VM, Furtenbacher T, Harrison JJ, Hartmann JM, Jolly A, Johnson TJ, Karman T, Kleiner I, Kyuberis AA, Loos J,Lyulin OM, Massie ST, Mikhailenko SN, Moazzen-Ahmadi N, Müller HSP, Naumenko OV, Nikitin AV, Polyansky OL, Rey M, Rotger M, Sharpe SW, Sung K, Starikova E, Tashkun SA, Vander Auwera J, Wagner G,Wilzewski J,Wcisło P, Yuh S, Zak EJ, The HITRAN 2016 molecular spectroscopic database. J Quant Spectrosc Radiat Transf 2017;203:3-69.

[3] Jacquinet-Husson N, Armante R, Scott NA, Chédin A, Crépeau L, Boutammine C, Bouhdaoui A, Crevoisier C, Capelle V, Boonne C,Poulet-Crovisier N, Barbe A, Benner DC, Boudon V, Brown LR,Buldyreva J, Campargue A, Coudert LH, Devi VM, Down MJ, Drouin BJ, Fayt A, Fittschen C, Flaud JM, Gamache RR, Harrison JJ, Hill C, Hodnebrog Ø, Hu SM, Jacquemart D, Jolly A, Jiménez E, Lavrentieva N, Liu AW, Lodi L, Lyulin OM, Massie ST, Mikhailenko S, Müller HSP, Naumenko OV, Nikitin A, Nielsen CJ, Orphal J, Perevalov V, Perrin A, Polovtseva E, Predoi-Cross A, Rotger M, Ruth AA, Shanshan Y, Sung K, Tashkun S, Tennyson J, Tyuterev VG, VanderAuwera J, Voronin B, Makie A.The 2009 edition of the GEISA spectroscopic database. J Mol Spectrosc 2016;327:31-72.

[4] Clerbaux C, Boynard A, Clarisse L, George M, Hadji-Lazaro J, Herbin H, Hurtmans D, Pommier M, Razavi A, Turquety S, Wespes C, Coheur PF. Monitoring of atmospheric composition using the thermal infrared IASI/MetOp sounder. Atmos Chem Phys 2009;9: 6041–54.

[5] Arimondo E, Glorieux P, Oka T. Radio-frequency spectroscopy inside a laser cavity; "pure" nuclear quadrupole resonance of gaseous CH_3I. Phys Rev A 1978;17:1375–93.

[6] Dubrulle A, Burie J, Boucher D, Herlemont F, Demaison J. Microwave spectra of methyl chloride, methyl bromide, and methyl iodide in the $v_6 = 1$ excited vibrational state, J Mol Spectrosc 1981;88:394–401.

[7] Paso R, Horneman VM, Anttila R. Analysis of the ν_1 Band of CH_3I. J Mol Spectrosc 1983;101:193-8.

[8] Wlodarczak G, Boucher D, Bocquet R, Demaison J. The rotational constants of methyliodide. J Mol Spectrosc 1987;124:53- 65.

[9] Alanko S, Horneman VM, Anttila R, Paso R. Overtone bands $2\nu_3$ of $^{12}CH_3I$ and $^{13}CH_3I$, J Mol Spectrosc 1990;141:149-166.

[10] Paso R, Alanko S. The effect of nuclear quadrupole hyperfine interaction on the IR absorption band ν_6 of $^{12}CH_3I$. J Mol Spectrosc 1993;157:122-131.

[11] Alanko S. A detailed analysis of the $\nu_2/\nu_5/\nu_3+\nu_6$ band system of $^{13}CH_3I$ and $^{12}CH_3I$. J Mol Spectrosc 1996;177:263-79.

[12] Carocci S, Di Lieto A, De Fanis A, Minguzzi, Alanko S, Pietila J. The Molecular Constants of $^{12}CH_3I$ in the Ground and $v_6 = 1$ Excited Vibrational State. J Mol Spectrosc 1998;191: 368-73.

[13] Haykal I, Doizi D, Boudon B, El Hilali A, Manceron L, Ducros G. Line positions in the $v_6=1$ band of methyl iodide: Validation of the C_{3v} TDS package based on the tensorial formalism. J Quant Spectrosc Radiat Transf 2016;173:13-9.

[14] Barrow GM, McKean DC. The intensities of absorption bands in the methyl halides. Proc Roy Soc London 1952;213A:27-41.

[15] Dickson AD, Mills IM, Crawford B. Vibrational intensities VIII. CH_3 and CD_3 chloride, bromide and iodide. J Chem Phys 1957;27:445-57.

[16] Sharpe S, Johnson T, Sams R, Chu RP, Rhoderick G, Johnson P. Gas-phase databases for quantitative infrared spectroscopy. Appl Spectrosc 2004; 58:1452– 61.

[17] Schneider W, Thiel W. Ab initio calculation of harmonic force fields and vibrational spectra for the methyl, silyl, germyl, and stannyl halides. J Chem Phys1987;86:923-35.

[18] Tudorie M, Foldes T, Vandaele AC, Vander Auwera J. CO_2 Pressure broadening and shift coefficients for the 1-0 band of HCl and DCl. J Quant Spectrosc Radiat Transf 2012;113:1092–101.

[19] Daneshvar L, Foldes T, Buldyreva J, Vander Auwera J. Infrared absorption by pure CO_2 near 3340 cm^{-1}: measurements and analysis of collisional coefficients and line-mixing effects at subatmospheric pressures. J Quant Spectrosc Radiat Transf 2014;149:258–74.

[20] Wells R. Rapid approximation to the Voigt/Faddeeva function and its derivatives. J Quant Spectrosc Radiat Transf 1999;62:29–48.

[21] Ballard J, Knight RJ, Vander Auwera J, Herman M, Di Lonardo G, Masciarelli G, Nicolaisen FM, Beukes JA, Christensen LK, McPheat R, Duxbury G, Freckleton R, Shine KP. An intercomparison of laboratory measurements of absorption cross-sections and integrated absorption intensities for HCFC-22. J Quant Spectrosc Radiat Transf 2000;66:109-28.

[22] De Bievre P, Holden NE, Barnes IL. Isotopic Abundances and Atomic Weights of the Elements. J. Phys. Chem. Ref. Data 1984;13:809-91.

[23] Anttila R, Paso R, Guelachvili G. A High-Resolution Infrared Study of the ν_4 Band of CH_3I. J Mol Spectrosc 1986;119:190-200.

[24] Alanko S, Horneman VM, Kauppinen J. The ν_3 Band of CH_3I around 533 cm^{-1}. J Mol Spectrosc 1989;135:76-83.

[25] Bray C, Perrin A, Jacquemart D, Lacome N. The ν_1, ν_4 and $3\nu_6$ bands of methyl chloride in the 3.4-μm region: Line positions and intensities. J Quant Spectrosc Radiat Transf 2011;112:2446-62.

[26] Flaud JM, Camy-Peyret C. Vibration-Rotation Intensities in H_2O-Type Molecules: Application to the $2\nu_2$, ν_1 and ν_3 Bands of H_2O. J Mol Spectrosc 1975;55:278-310.

[27] KwabiaTchana F, Kleiner I, Orphal J, Lacome N, Bouba O. New analysis of the Coriolis-interacting ν_2 and ν_5 bands of $CH_3{}^{79}Br$ and $CH_3{}^{81}Br$. J Mol Spectrosc 2004;228:441-52.

[28] Tarrago G. The frequencies of vibration-rotation transitions of molecules with ternary axis of symmetry; calculation of the corrections to fourth order. Can. J. Phys 1965;19:149-217.

[29] Tarrago G, Delaveau M. Triad $\nu_n(A_1)$, $\nu_t(E)$, $\nu_{t'}(E)$ in C_{3v} molecules: Energy and intensity formulation (Computer Programs). J Mol Spectrosc 1986;119:418-25.

[30] Bowater IC, Brown JM, Carrington A. Microwave spectroscopy of nonlinear free radicals - I. General theory and application to the Zeeman effect in HCO. Proc R Soc Lond A 1973;333;265-88.

[31] Gordy W, Cook RL, Microwave molecular spectra, John Wiley and sons, New York (1984).

[32] Hoffman KJ, Davies PB. Pressure broadening coefficients of ν_5 fondamental band lines of CH_3I at 7 µm measured by diode laser absorption spectroscopy. J Mol Spectrosc 2008;252:101-7.

[33] Flaud JM, Brizzi G, Carlotti M, Perrin A, Ridolfi M. MIPAS database: Validation of HNO_3 line parameters using MIPAS satellite measurements. Atmos Chem Phys 2006;6: 1–12.

[34] Owens A, Yurchenko SN, Yachmenev A, Tennyson J, Thiel W. A global *ab initio* dipole moment surface for methyl chloride. J Quant Spectrosc Radiat Transf 2016;184:100-10.

[35] Owens A, Yurchenko YN, Yachmenev A, Tennyson J, Thiel W. The accurate *ab initio* vibrational energies of methyl chloride. J Chem Phys 2015;142:244306.

Table 1

Pressure of CH_3I (in hPa) and number of interferograms averaged to yield the corresponding spectrum (# scans). All the spectra were recorded with an absorption path length of 12.4 ± 0.1 cm, at a stabilized room temperature of 295 ± 1 K, a resolution (equal to 0.9 divided by the maximum optical path difference) of 0.0019 cm^{-1} and an entrance aperture diameter of the interferometer equal to 1.5 mm. The absolute uncertainty on the pressure is equal to 0.5% of the value given.

#	$P(CH_3I)$	# scans
S1	3.406 (17)	840
S2	6.433 (32)	828
S3	8.611 (43)	900
S4	11.418 (57)	940
S5	14.28 (7)	880
S6	21.28 (11)	900
S7	28.70 (15)	1040

Table 2:

(A) Transition moment constants for the $2\nu_3$ and ν_6 bands.

Band	Constants		Value in Debye
$2\nu_3$	${}^{33}\mu_0^{\Delta\ell=0}$	φ_z	$\pm 6.84 \times 10^{-3}$ [$]
ν_6	${}^{6}\mu_0^{\Delta\ell=\pm1}$	φ_x	$6.14936(700) \times 10^{-2}$
	${}^{6}\mu_4^{\Delta\ell=\pm1}$	$\{i\varphi_y, J_z\}$	$-1.4331(990) \times 10^{-4}$
	${}^{6}\mu_5^{\Delta\ell=\pm1}$	$\{\varphi_z, iJ_y\}$	$-7.96(150) \times 10^{-5}$

(B) Statistical analysis for the line intensity calculation:

Number of lines	840
Percentage of lines	
0% ≤δ< 8%	65.6 %
8% ≤δ< 16%	23.0%
16% ≤δ< 30%	11.4%

$\delta = |I_{Obs} - I_{Calc}| / I_{Obs}$ in %

φ_x, φ_y and φ_z stands for the direction cosines Φ_{Zx} , Φ_{Zy} and Φ_{Zz}, respectively.

1 Debye = 3.22564×10^{-30} Coulomb m. The quoted errors are one standard deviation.

[$] Maintained at this value during the calculation.

Table 3

Results of the intensity computation at 296 K (for a pure isotopic sample of $^{12}CH_3I$)

Band	Number of lines	Number of lines	Band intensity	Int_{Max}	Sigma Min	Sigma Max	J_{Max}	K_{Max}
	Hyp	No Hyp	$\times 10^{-19}$	$\times 10^{-23}$				
ν_6	16573	12394	12.4	250	705.15	1102.43	88	24
$2\nu_3$	6331	5227	0.183	3.8	986.53	1076.68	88	21
Total	23157	17890	1.26					

"Hyp" and "No Hyp" identify the number of lines generated when accounting and not accounting for the hyperfine structure, respectively. "Band intensity" and "Int_{Max}" (maximum value of the computed line intensities) are in cm^{-1}/(molecule cm^{-2}). "Sigma Min" and "Sigma Max" are the minimum and maximum values of the computed line positions (in cm^{-1}), respectively.

Table 4

Status of the previous band intensity measurements or calculations.

Results of the present line intensity computation at 296 K for the quoted cold bands (ν_6 and $2\nu_3$ respectively) together with their associated hot bands (see Eq. 9) and for a natural sample of CH_3I.

Band	Integrated band intensity in $cm^{-1}/(molecule \times cm^{-2})$	Method	Ref.
ν_6	$0.150(2)\times10^{-17}$	Low resolution integrated intensities	[15]
ν_6	$0.150(2)\times10^{-17}$	Low resolution integrated intensities	[16]
ν_6	0.322×10^{-17}	*Ab initio* calculation	[17]
ν_6	0.138×10^{-17}	Computation of the ν_6 line intensities for the whole band$ and estimation of the hot band contribution using Eq. (9)	This work
$2\nu_3$	0.19×10^{-19}	Low resolution integrated intensities	[16]
$2\nu_3$	~ 0.20×10^{-19}	Computation of the $2\nu_3$ line intensities for the whole band* and estimation of the hot band contribution using Eq. (9)	This work

$ For the ν_6 band, the line intensity parameters were derived through a least square fit performed on the set of individual line by line intensity measurement (see Table 2).

* For the $2\nu_3$ band, the line intensity parameters were estimated from the PNNL band intensity data.

List of figures

Figure 1

Results of the multi-spectrum analysis applied to 7 spectra (S1 to S7) of a small part of the v_6 band of CH_3I. The top panel shows the observed spectra and the lower panel presents the best-fit residuals corresponding to spectra S1 to S7. For the spectral range in Figure 1, the transitions considered for the line intensity computation are listed in Annex 2. Please note that the 915.538 cm^{-1} line, which corresponds to a blended line cluster was not taken into account for the line intensity computation.

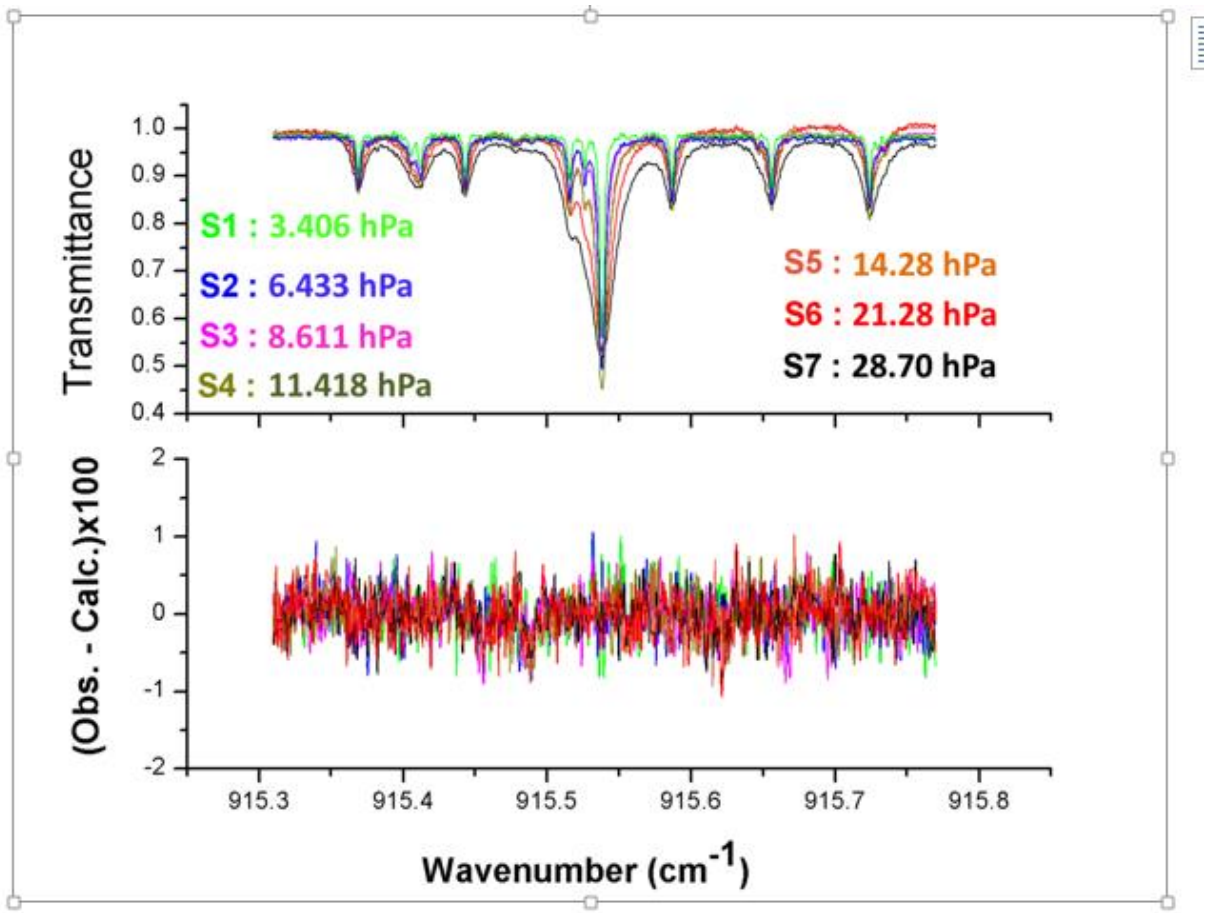

Figure 2

Comparison between various sources of relative uncertainty on the measured intensities of 3 selected lines of high, medium and low intensity: $^{R}R(26,0)$, $^{P}P(30,4)$ and $^{P}P(57,4)$.

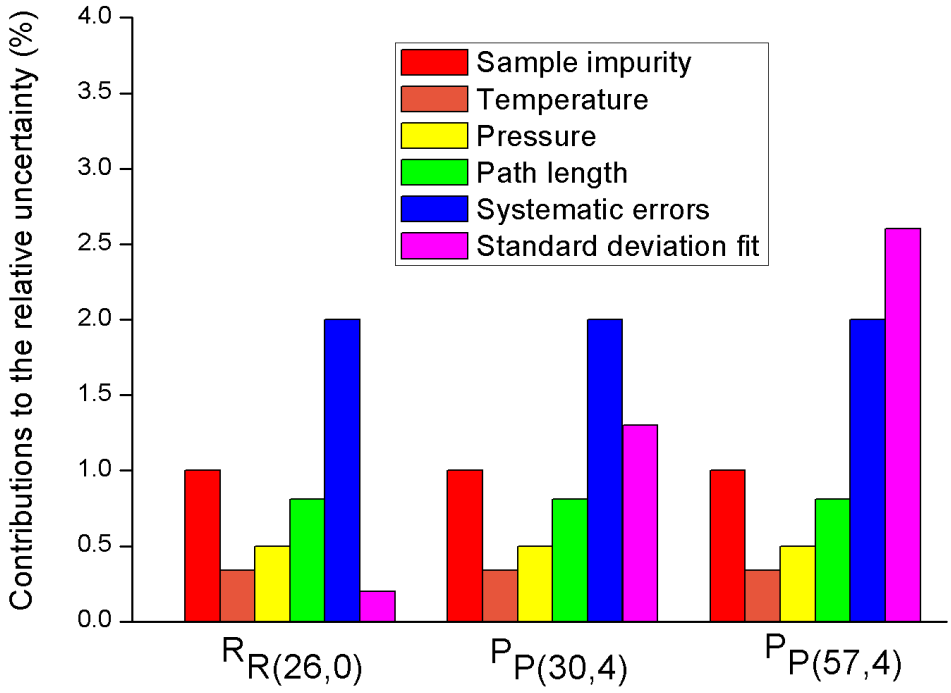

Figure 3

Residuals (Obs–Calc)/Obs (in %) of the line intensity calculation for ν_6 line intensities plotted as a function of the experimental line intensities.

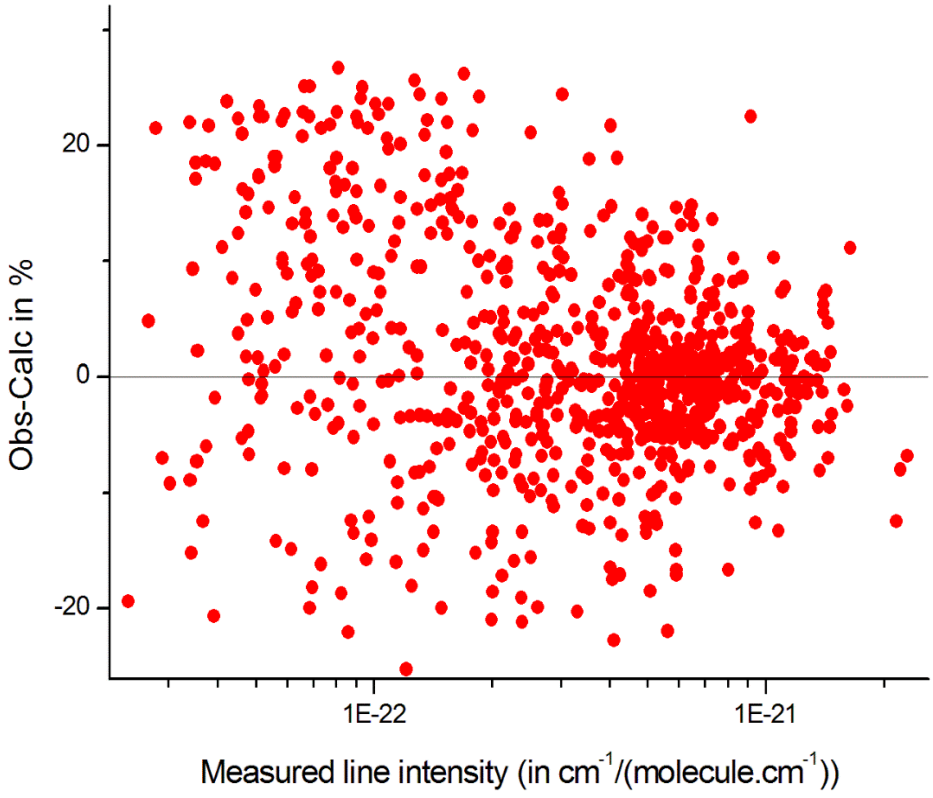

Figure 4

Portion of the CH_3I spectrum near the origin of the $^{R}Q_{K=3}$ lines structure of the ν_6 band in the 909.1 cm^{-1} region. The observed spectrum is spectrum S3 in Table 1. The calculated spectrum was generated considering the self-broadening coefficients of the lines measured in this work. For the low J lines, it is obvious that accounting for the hyperfine structure ["Calc. (with HPFS)"] leads to a better agreement with observation than when this effect is not considered during the calculation ["Calc. (no HPFS)"].

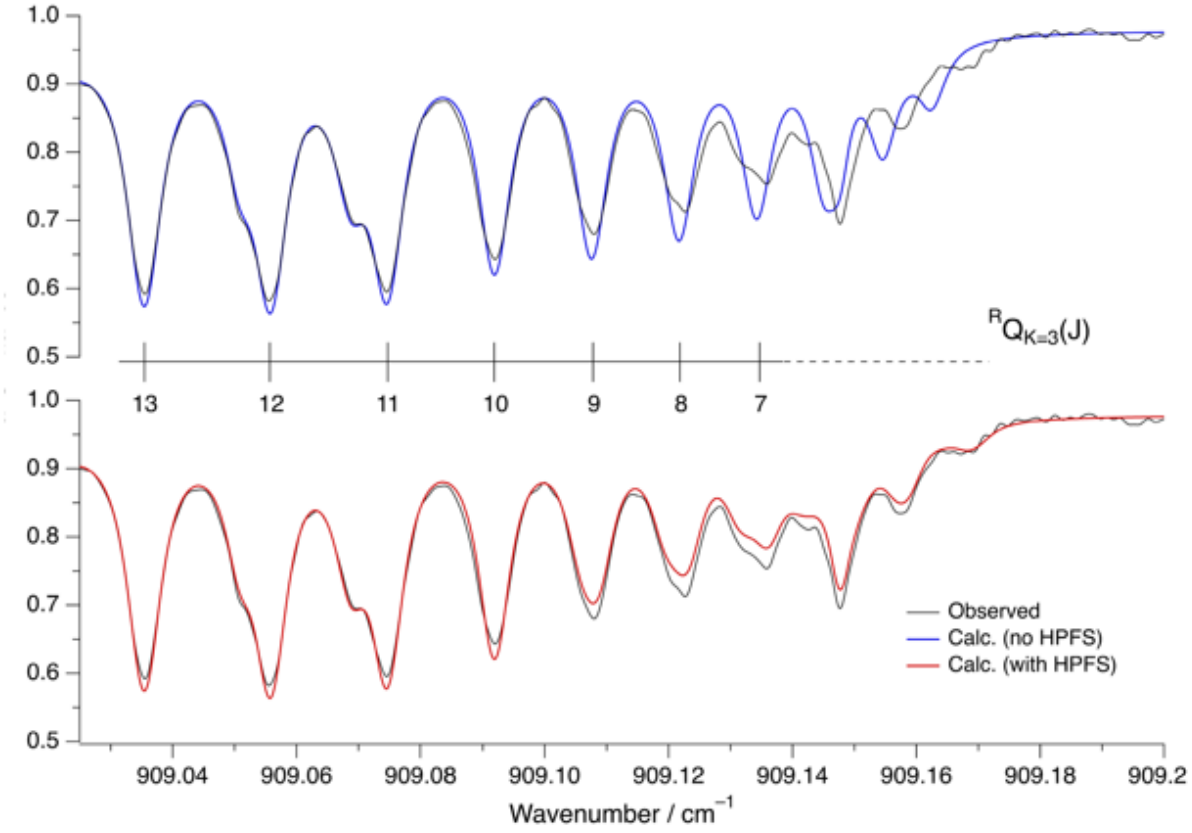

Figure 5

Comparison with the Pacific Northwest National Laboratory (PNNL) [16] absorption cross sections in the ν_6 band region (see text for details).

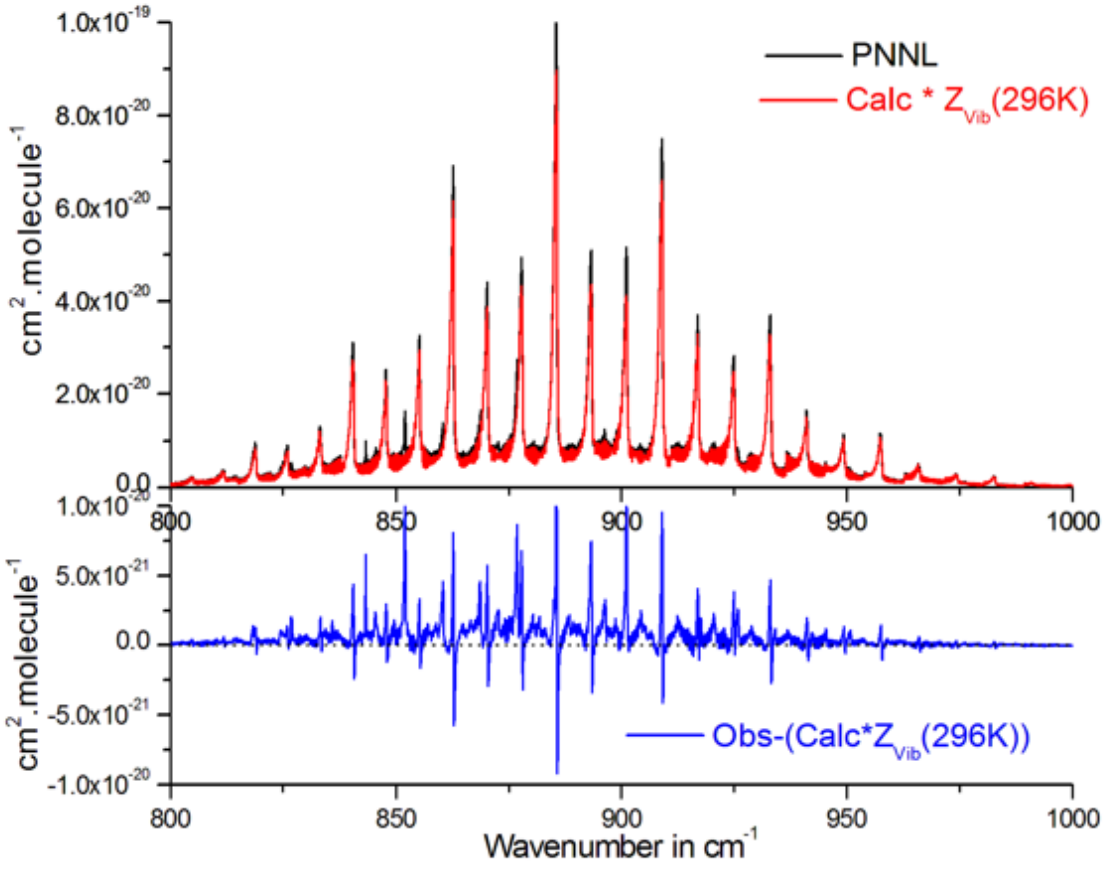

Figure 6

Same as Fig. 5, applied to the $2\nu_3$ band region.